



Breast MRI during lactation: effects on tumor conspicuity using dynamic contrast-enhanced (DCE) in comparison with diffusion tensor imaging (DTI) parametric maps

Noam Nissan^{1,2} · Tanir Allweis³ · Tehillah Menes⁴ · Asia Brodsky⁵ · Shani Paluch-Shimon⁶ · Ilana Haas⁷ · Orit Golan⁸ · Yaheli Miller³ · Hani Barlev⁹ · Einat Carmon¹⁰ · Malka Brodsky¹ · Debbie Anaby¹ · Philip Lawson¹ · Osnat Halshtok-Neiman¹ · Anat Shalmon¹ · Michael Gotlieb¹ · Renata Faermann¹ · Eli Konen¹ · Miri Sklair-Levy¹

Received: 3 April 2019 / Revised: 12 July 2019 / Accepted: 27 August 2019 / Published online: 16 September 2019
© European Society of Radiology 2019

Abstract

Purpose To investigate the effect of lactation on breast cancer conspicuity on dynamic contrast-enhanced (DCE) MRI in comparison with diffusion tensor imaging (DTI) parametric maps.

Materials and methods Eleven lactating patients with 16 biopsy-confirmed pregnancy-associated breast cancer (PABC) lesions were prospectively evaluated by DCE and DTI on a 1.5-T MRI for pre-treatment evaluation. Additionally, DCE datasets of 16 non-lactating age-matched breast cancer patients were retrospectively reviewed, as control. Contrast-to-noise ratio (CNR) comprising two regions of interests of the normal parenchyma was used to assess the differences in the tumor conspicuity on DCE subtraction images between lactating and non-lactating patients, as well as in comparison against DTI parametric maps of λ_1 , λ_2 , λ_3 , mean diffusivity (MD), fractional anisotropy (FA), and maximal anisotropy index, λ_1 – λ_3 .

Results CNR values of breast cancer on DCE MRI among lactating patients were reduced by 62% and 58% ($p < 0.001$) in comparison with those in non-lactating patients, when taking into account the normal contralateral parenchyma and an area of marked background parenchymal enhancement (BPE), respectively. Among the lactating patients, DTI parameters of λ_1 , λ_2 , λ_3 , MD, and λ_1 – λ_3 were significantly decreased, and FA was significantly increased in PABC, relative to the normal lactating parenchyma ROIs. When compared against DCE in the lactating cohort, the CNR on λ_1 , λ_2 , λ_3 , and MD was significantly superior, providing up to 138% more tumor conspicuity, on average.

Conclusion Breast cancer conspicuity on DCE MRI is markedly reduced during lactation owing to the marked BPE. However, the additional application of DTI can improve the visualization and quantitative characterization of PABC, therefore possibly suggesting an additive value in the diagnostic workup of PABC.

Eli Konen and Miri Sklair-Levy are authors of equal contribution.

Electronic supplementary material The online version of this article (<https://doi.org/10.1007/s00330-019-06435-x>) contains supplementary material, which is available to authorized users.

✉ Noam Nissan
noamniss@gmail.com

¹ Department of Radiology, Sheba Medical Center, Emek Ha-Ella 1 st., 5265601 Tel Hashomer, Israel

² Sackler School of Medicine, Tel Aviv University, Tel Aviv, Israel

³ Department of General Surgery, Kaplan Medical Center, Rehovot, Israel

⁴ Department of General Surgery, Tel Aviv Souraski Medical Center, Tel Aviv, Israel

⁵ Department of General Surgery, Bnai Zion Medical Center, Haifa, Israel

⁶ Department of Oncology, Shaare Zedek Medical Center, Jerusalem, Israel

⁷ Department of General Surgery, Meir Medical Center, Saba, Israel

⁸ Department of Radiology, Tel Aviv Souraski Medical Center, Tel Aviv, Israel

⁹ Department of General Surgery, Laniado Medical Center, Netanya, Israel

¹⁰ Department of General Surgery, Hadassah Medical Center, Jerusalem, Israel

Key Points

- Breast cancer conspicuity on DCE MRI has decreased by approximately 60% among lactating patients compared with non-lactating controls.
- DTI-derived diffusion coefficients and the anisotropy indices of PABC lesions were significantly different than those of the normal lactating fibroglandular tissue.
- Among lactating patients, breast cancer conspicuity on DTI-derived parametric maps provided up to 138% increase in contrast-to-noise ratio compared with DCE imaging.

Keywords Breast · Lactating · Breastfeeding · Diffusion · Magnetic resonance imaging

Abbreviations

ADC	Apparent diffusion coefficient
BPE	Background parenchymal enhancement
CNR	Contrast-to-noise ratio
DCE	Dynamic contrast-enhanced
DCIS	Ductal carcinoma in situ
DTI	Diffusion tensor imaging
FA	Fractional anisotropy
FOV	Field of view
IDC	Invasive ductal carcinoma
ILC	Invasive lobular carcinoma
MD	Mean diffusivity
PABC	Pregnancy-associated breast cancer
ROI	Region of interest
TE	Echo time
TR	Repetition time

Introduction

During pregnancy and lactation, the breast undergoes notable physiological and morphological transformations, resulting in an enlargement in size and in a redistribution of its composing elements characterized by glandular proliferation and involution of the stromal and adipose tissues [1]. Ultimately, the lactating breast demonstrates increased vascularity and higher parenchymal density and associated palpable nodularity, making both clinical examination and radiological evaluation more challenging [2].

Breast cancer that is diagnosed during pregnancy, during lactation, or during the first year post-partum is defined as pregnancy-associated breast cancer (PABC). PABC accounts for ~ 1% of all breast cancer cases, though its incidence is on the rise [3]. It is often diagnosed only after the appearance of clinical symptoms, usually as a palpable breast mass. Then, it is associated with an advanced disease and carries poor prognosis [4].

During lactation, initial radiological workup of the breast leans mostly on ultrasound (US). Mammography utility is relatively limited, due to the high parenchymal density [5]. Yet, when malignancy is suspected or proven, assessment of underlying micro-calcifications by mammography may be beneficial [4]. Currently, the role of breast MRI during

lactation is controversial, both as a screening modality for high-risk patients such as BRCA carriers and for diagnostic purposes. The use of gadolinium is considered safe during lactation [6]; however, the utility of dynamic contrast-enhanced (DCE) MRI is limited because lactating parenchyma exhibits increased vascular permeability, associated with marked background parenchymal enhancement (BPE) in the derived images [7–10]. Lactation-induced BPE elevates the challenge of differentiating between suspicious findings and lactation-induced changes. Consequently, concerns are raised with regard to DCE utility in PABC owing to reduced tumor conspicuity and limited sensitivity in detecting small enhancing masses and non-mass enhancement [11, 12].

An alternative MRI modality to DCE may be the diffusion-weighted imaging (DWI) techniques, which provide a non-perfusion-based contrast between malignant and normal tissues, stemming from changes in the water diffusivity. Foremost, the DWI-derived apparent diffusion coefficient (ADC) maps were shown to be a useful tool alongside DCE in breast MRI [13]. Moreover, in recent years, diffusion tensor imaging (DTI), an advanced diffusion-based modality, was introduced in breast imaging [14–17]. It provides quantitative structural information through maps of anisotropy indices and diffusion coefficients [18]. DTI properties of healthy breasts were reported by several studies [14, 19–21], including during lactation [22] and post-weaning [23]. Furthermore, DTI parametric maps were shown to be useful in breast cancer characterization [15–17, 24–29] as well as in monitoring response to neo-adjuvant chemotherapy (NAC) [30, 31]. In contrast to DCE, diffusion-based MRI does not rely on vascularity properties thus might be immune to the lactation-related BPE drawbacks of DCE. Therefore, our goal was to investigate whether DTI, as a supplementary technique to the conventional DCE MRI breast protocol, may improve the tumor conspicuity among lactating patients with breast cancer.

Materials and methods

Protocols were approved by the institutional Internal Review Board of Sheba Medical Center and a signed informed consent was obtained from all participants.

Patients

Eleven lactating participants (median age, 34 years; range, 30–45 and median breastfeeding duration, 9 months; range, 1–16) were prospectively recruited in eight nationwide breast care centers and referred to participate in this single-center study between December 2016 and November 2018. All subjects were newly diagnosed, biopsy-confirmed breast cancer ($n = 16$ lesions) patients, scanned for pre-treatment evaluation. All PABCs were invasive ductal carcinoma (IDC), except for one ductal carcinoma in situ (DCIS) (median lesion size of 21 mm; range, 8–98 mm). Complete subject characteristics are summarized in Table 1. For the quantification of the lactation effect on tumor conspicuity, a control group of 16 non-lactating pre-menopausal patients with newly diagnosed breast cancer was retrospectively analyzed. These patients were retrieved through the institutional radiology information system (RIS) by identifying reports of such patients who underwent pre-treatment MRI throughout 2017. The control group (median age, 36.5 years) comprised of 14 IDC patients (range, 31–40 years), one DCIS and one invasive lobular carcinoma (ILC). The median lesion size was 21 mm with a range of 8–36 mm.

MRI protocol

All scans were performed in a single center on a 1.5-T (Signa Excite HDX, GE Healthcare) scanner with a dedicated double breast coil with eight channels. The MRI protocol included an axial vibrant multi-phase 3D DCE T1-weighted scan using

echo time (TE)/repetition time (TR) = 2.6/5.4 ms, flip angle, 15; bandwidth, 83.3 kHz; matrix, 512×364 ; field of view (FOV), 340 mm; and slice thickness, 2 mm. DCE was acquired prior to and four times after an automatic injection of contrast agent bolus (0.1 ml/kg at 2 ml/s Dotarem, (gadoterate meglumine)) followed by a 20-ml saline flush, with total duration 07:35 min (1:25 min per dynamic scan). Non-fat-suppressed axial fast 2D T2-weighted images were acquired using TE/TR = 88/5480 ms with in-plane resolution of $0.9 \times 0.8 \text{ mm}^2$ (FOV 340 mm). For the lactation group only, axial fat-suppressed (frequency-selective) DTI was acquired prior to DCE, using spin-echo echo-planar-imaging (SE-EPI) with 32 diffusion directions; b values of 0 and 700 s/mm^2 ; TE/TR = 91/1700 ms; and in-plane resolution of $1.9 \times 2.6 \text{ mm}^2$ (FOV 340 mm), during 09:38 min. In both T2 and DTI protocols, 72 slices were acquired with slice thickness of 2.5 mm. Lactating patients were consulted to pump breast milk prior to the scan and avoid breastfeeding in the following hours.

DTI processing

The diffusion tensor parameters were calculated and mapped pixel-by-pixel for each given slice using proprietary software developed at the Weizmann Institute of Science and granted for use by permission. The software fits the diffusion data according to the Stejskal-Tanner equation and yields tensor parameters: three principal eigenvalues, λ_1 , λ_2 , λ_3 , mean diffusivity (MD, mean of the three eigenvalues) and two anisotropy indices, maximal anisotropy index $\lambda_1 - \lambda_3$ and fractional anisotropy (FA) [18]:

presenting symptoms, tumor's maximal diameter per λ_1 map and DCE subtraction image (mm), as well as pathological results

Table 1 Demographic, clinical, MRI, and pathology characteristics of PABC cohort. Characteristics of 11 PABC patients with 16 lesions are summarized, including age (years), breastfeeding duration (months),

Subject	Age	Duration	Presentation	DTI	DCE	Pathology
1a	30	3	Palpable mass	27	23	IDC grade III (ER+, PR-, HER2+)
1b				16	16	
2a	33	3	Palpable mass	36	35	IDC grade III
2b				17	20	
2c				13	12	
3	36	1	Palpable mass	29	26	IDC grade III+DCIS
4	31	14	Palpable mass, milk rejection	13	15	IDC grade III (ER+, PR+, HER2-)
5a	45	13	Palpable mass	7	8	IDC grade III (ER+, PR+, HER2-)
5b				16	15	
6a	36	14	Palpable mass	9	9	IDC (ER+, PR+, HER2+)
6b				27	21	
7	36	16	Palpable mass	16	16	IDC grade III (ER+, PR-, HER2-)
8	32	9	Palpable mass, mastalgia	75	73	IDC triple negative
9	34	1	Palpable mass	24	25	IDC grade III+DCIS (triple neg.)
10	38	10	Palpable mass	60	54	DCIS high-grade
11	34	9	Palpable mass	65	98	IDC+DCIS

$$FA = \frac{\sqrt{3[(\lambda_1 - \langle \lambda \rangle)^2 + (\lambda_2 - \langle \lambda \rangle)^2 + (\lambda_3 - \langle \lambda \rangle)^2]}}{\sqrt{2(\lambda_1^2 + \lambda_2^2 + \lambda_3^2)}}$$

Image analysis

The reporting radiologists (NN and MSL) with 8 and 19 years of experience in breast MRI, respectively, analyzed all of the exams together by consensus and were not blinded to the clinical reports.

DCE analysis The newly diagnosed biopsy-confirmed lesions were identified on DCE subtraction images in agreement with the clinical and conventional radiological localization. Lesion's size was determined based on the longest diameter measured on the axial image and regions of interest (ROIs) of the tumor were manually delineated, excluding apparent necrotic tissue, using commercial PACS (picture archiving and communication system) workstation analysis tools (Algotec). Due to the heterogeneous BPE distribution [7, 8], two separate ROIs of the normal contralateral lactating fibroglandular tissue were measured (the same size as the tumor): ROI_{normal}, chosen in the corresponding area of the same slice of the contralateral breast; ROI_{BPE}, chosen in the contralateral breast but not in the same slice, where the BPE was most marked. A representative DCE analysis of the three ROIs is illustrated in Supplementary Figure 1. Contrast-to-noise ratio (CNR) was quantified as a tumor conspicuity measure using the following equation [32]:

$$CNR = \frac{\mu_{\text{tumor}} - \mu_{\text{tissue}}}{\sqrt{\sigma_{\text{tumor}}^2 + \sigma_{\text{tissue}}^2}}$$

where μ_{tumor} and μ_{tissue} are defined as the mean signal intensity of the investigated lesion and the normal lactating fibroglandular tissue, respectively. Noise was defined as the standard deviation of intensities, σ_{tumor} and σ_{tissue} in both ROIs. Consequently, two sets of CNR values are provided: CNR_{normal} and CNR_{BPE}.

DTI analysis In order to exclude noisy non-fat-suppressed pixels with non-physiological decreased diffusivity due to partial volume effect in the tissue-fat interface, a case-by-case adjustment of the b0 signal intensity (SI) threshold was applied, using the matched T2-weighted image as anatomical reference [33]. Lesion size was measured on thresholded λ_1 maps, based on the longest diameter. ROIs of the tumor were manually delineated on color-coded λ_1 maps using a threshold of diffusivity $< 1.7 \times 10^{-3} \text{ mm}^2/\text{s}$ in a central slice of the depicted tumor, as was previously reported to be the optimal

cutoff for differentiating between malignant and benign lesions [15], in accordance with their localization on DCE subtraction images. Similar to the DCE analysis, two matching ROIs of normal fibroglandular tissue were manually drawn on the λ_1 map, representing the corresponding normal parenchymal diffusivity: ROI_{normal} and ROI_{BPE} as defined in the “DCE analysis” section. Likewise, two DTI-derived CNR values were measured: CNR_{normal} and CNR_{BPE}, respectively. All DTI parameters were given as the means, standard deviations (SD), medians, and interquartile range (IQR) values.

Statistical analysis

The normality of the distribution of the DTI parameters was tested using the Shapiro-Wilk test. Unpaired two-tailed Student's *t* tests were applied for evaluating differences between CNR values of DCE among lactating and non-lactating controls, for the two ROIs. Paired two-tailed Student's *t* tests were applied for evaluating intra-individual differences between CNR of DCE and DTI parameters and between pairs of DTI parameters, among the lactating cohort, for the two ROIs. Pearson's correlation test (Excel 2010, Microsoft) was applied to measure the agreement between λ_1 based on the longest tumor diameter and DCE. Statistical significance was defined as $p < 0.05$.

Results

CNR comparison between lactating and non-lactating groups using DCE

All known newly diagnosed PABC lesions ($n = 16$), as well as lesions of the non-lactating control group ($n = 16$), were visible on DCE subtraction images, exhibiting higher signal intensity as compared with the surrounding parenchymal enhancement. Representative DCE subtraction images of lactating and non-lactating breast cancer patients demonstrate the pronounced BPE difference, which is more evident in the former group (Fig. 1). By comparing the means of CNR_{normal} and CNR_{BPE} calculated on DCE subtraction images for the two pre-menopausal groups, lactating and non-lactating, quantification of the observed reduction in tumor conspicuity during lactation was obtained; relatively high CNR measurements were calculated for the non-lactating control group, with CNR_{normal} = 3.64 ± 0.77 and CNR_{BPE} = 1.97 ± 0.68 , whereas dramatic decline was observed among the lactating cohort, with CNR_{normal} = 1.40 ± 0.39 and CNR_{BPE} = 0.82 ± 0.49 , corresponding to 62% and 58% relative reduction in tumor's conspicuity during the lactation period. Results are presented in Fig. 1.

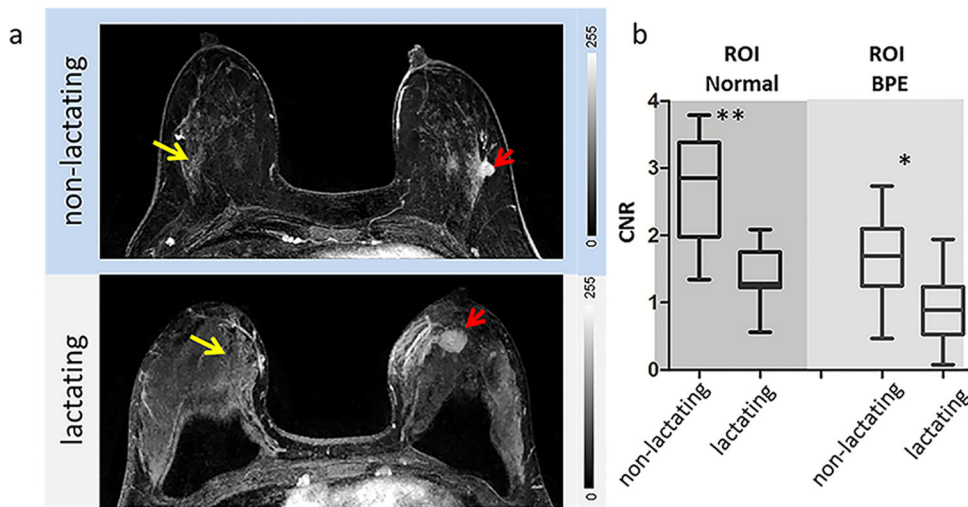


Fig. 1 CNR comparison between lactating cohort and non-lactating control groups. **a** A representative DCE subtraction MIP image of a 36-year-old non-lactating patient with IDC and a 31-year-old lactating patient with silicone implants and IDC. DCE image scale is in arbitrary units (0–255). The lesions could be identified on both images (red arrowhead), though a considerable BPE is exhibited in the lactating breast (yellow arrow), reducing the tumor conspicuity ($CNR_{reciprocal} = 1.22$ and $CNR_{BPE} = 0.6$

for the lactating patient and $CNR_{reciprocal} = 3.09$ and $CNR_{BPE} = 1.88$ for the non-lactating patient). **b** CNR results of the lactating and the non-lactating groups are demonstrated in box (median \pm interquartile range [IQR]) and whisker (± 1.5 IQR) plots ($n = 16$). Statistically significant changes were found between the two groups, for the datasets of the normal contralateral ROIs (** $p = 0.0002$) and the BPE ROIs (* $p = 0.001$), as obtained by an unpaired two-tailed Student’s *t* test

DTI of the lactating breast

DTI analysis provided tissue characterization of the normal lactating fibroglandular tissue, as well as tumor depiction. Predominantly, the lactating breast presented relatively low values of diffusivity and anisotropy. MD maps along with a breast illustration and an anatomical reference are presented in Fig. 2, highlighting the pronounced ductal microstructure in the sub-areolar area. The breast diffusivity is markedly heterogeneous, with two distinct diffusivity areas: high diffusivity in the central sub-areolar area and decreased diffusivity, though in the normal range, in the

posterior-peripheral area. This wide variance is further reflected in the DTI parameter results for the two ROIs measured in the contralateral breast (ROI_{normal} , ROI_{BPE}), as summarized in Table 2. DTI measurements in the tumor ROI yielded statistically significant differences in all DTI parameters (Table 2). In agreement with their localization on the DCE subtraction images, all lesions were visible on the corresponding slices in the λ_1 maps. Comparison of the lesion’s diameter on DCE and λ_1 maps showed high congruence ($r = 0.94$, $p < 0.0001$). Representative images of DCE and DTI of PABC of three different lactating patients are given in Figs. 3, 4, and 5.

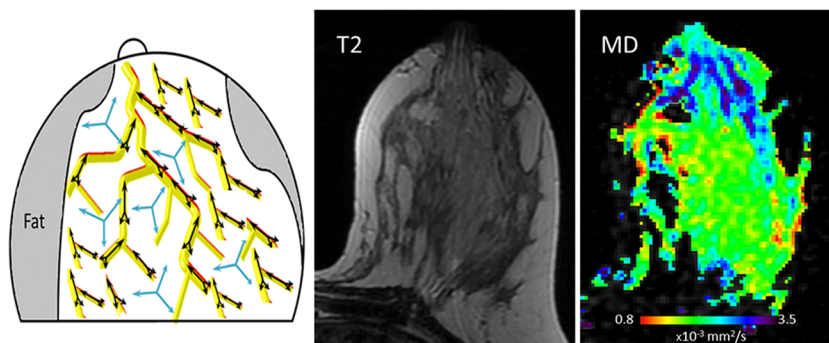


Fig. 2 Illustration of breast microstructural diffusivity, anatomic T2-weighted image, and DTI-derived mean diffusivity map of the normal lactating breast. Illustration of the breast microstructure, showing the surrounding fat and the fibroglandular tissue. The fibroglandular tissue is composed of the ductal tree (yellow) and connective tissue (blue). Anatomical T2-weighted image and DTI-derived mean diffusivity map of the normal lactating breast (contralateral) of a 38-year-old PABC patient are also presented. On the T2-weighted image, the fat appears

brighter than the fat-rich milky, fibroglandular tissue. Also, the central ducts in the nipple region are visible. A further characterization of the breast microstructure is given by MD parametric map, where increased diffusivity in a ductal shaped configuration is exhibited in the central sub-areolar region, and relatively decreased diffusivity is exhibited in the breast periphery, reflecting the change in the ducts’ diameter in these regions

Table 2 DTI parameters of lactating patients. Mean and SD of average values calculated for each subject, per ROI. Normal breast was measured in two areas, ROI_{normal} and ROI_{BPE}, on the contralateral non-affected

breast. Paired *p* value accounts for intra-individual comparison for between normal and malignant tissues. λ_1 , λ_2 , λ_3 , MD, and λ_1 – λ_3 are in units of $\times 10^{-3}$ mm²/s

		λ_1	λ_2	λ_3	MD	FA	λ_1 – λ_3
PABC (<i>n</i> = 16)	Mean \pm SD	1.17 \pm 0.11	0.95 \pm 0.11	0.74 \pm 0.11	0.95 \pm 0.11	0.25 \pm 0.05	0.43 \pm 0.07
	Range	1.02–1.36	0.85–1.17	0.58–1.03	0.82–1.17	0.12–0.31	0.28–0.57
ROI _{normal} (<i>n</i> = 16)	Mean \pm SD	2.05 \pm 0.26	1.71 \pm 0.24	1.40 \pm 0.30	1.72 \pm 0.24	0.19 \pm 0.09	0.65 \pm 0.29
	Range	1.73–2.45	1.36–2.11	0.82–1.86	1.38–2.13	0.08–0.43	0.29–1.54
<i>p</i> value		< 0.0001	< 0.0001	< 0.0001	< 0.0001	< 0.05	< 0.005
ROI _{BPE} (<i>n</i> = 11)	Mean \pm SD	1.98 \pm 0.22	1.69 \pm 0.20	1.44 \pm 0.20	1.99 \pm 0.14	0.16 \pm 0.05	0.54 \pm 0.15
	Range	1.80–2.32	1.48–2.01	1.18–1.80	1.51–2.04	0.09–0.25	0.30–0.77
<i>p</i> value		< 0.0001	< 0.0001	< 0.0001	< 0.0001	< 0.005	< 0.05

Tumor conspicuity in DCE and DTI among lactating patients

In all lactating patients, the tumors were identified in DCE subtraction images, though with limited tumor conspicuity due to the prominent BPE surrounding the tumor and in the contralateral breast. Tumor conspicuity was found to be improved in DTI parametric maps λ_1 (Figs. 3, 4, and 5) and MD (Fig. 3). Low maximal anisotropy (λ_1 – λ_3) values appear in the tumor ROIs as well as in wide areas of the normal fibroglandular tissue in both breasts, stressing the poor tumor conspicuity of this parameter during lactation and its inferior specificity (Fig. 3). Furthermore, an automatic segmentation was enabled by setting a threshold of $\lambda_1 > 1.7 \times 10^{-3}$ mm²/s, despite scattered noisy pixels in the normal lactating fibroglandular tissue, especially in the tissue-fat interface

where partial volume effect exists (Figs. 3, 4, 5, and 6). When evaluating DTI maps in the corresponding areas with marked BPE, the diffusivity maps were useful in excluding contralateral disease, as shown by the λ_1 map in Fig. 6.

Overall, according to the CNR_{normal} calculation, DTI-derived tumor conspicuity values of λ_1 , λ_2 , and MD (1.94 \pm 0.44, 1.90 \pm 0.60, 2.00 \pm 0.56, respectively) maps were significantly superior to those of DCE images (1.40 \pm 0.39) (*p* < 0.05, *p* < 0.005, *p* < 0.0001, respectively). No significant change was found between λ_1 and MD (*p* = 0.35) maps. For the CNR_{BPE} measurements, even higher tumor conspicuity values were found for λ_1 , λ_2 , λ_3 , and MD (1.81 \pm 0.67, 1.95 \pm 0.87, 1.79 \pm 0.83, respectively) maps as compared with those of DCE images (0.82 \pm 0.49) (*p* < 0.005, for all). These results correspond to an increase by up to 43% for CNR_{normal} and by up to 138% for CNR_{BPE} by DTI-derived parameters, in

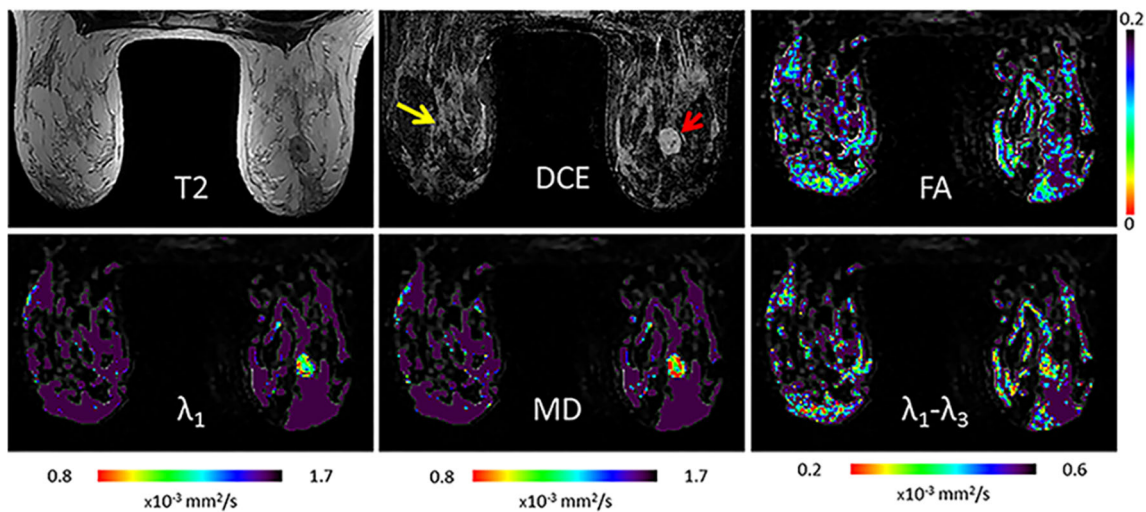


Fig. 3 T2, DCE, and DTI parametric maps of PABC patient. Representative images of a 36-year-old lactating patient with newly diagnosed 16-mm IDC: T2-weighted image, DCE subtraction image, and DTI-derived parametric maps of λ_1 , MD, FA, and λ_1 – λ_3 are presented. Pixels above the diffusivity threshold (with λ_1 and MD values $> 1.7 \times 10^{-3}$ mm²/s and λ_1 – λ_3 values $> 0.6 \times 10^{-3}$ mm²/s) are colored in purple, whereas pixels below the threshold are colored according to the

parametric scale. The lesion appears hypointense on the T2 image. In the DCE image, the tumor could be depicted (red arrowhead), though on top of non-negligible BPE in both breasts (yellow arrow). Instead, in λ_1 and MD, the tumor is clearly visible with increased parametric contrast vs. the normal lactating fibroglandular tissue. However, in this case, the FA map does not reveal the tumor localization while the tumor's decrease in λ_1 – λ_3 values is non-specific

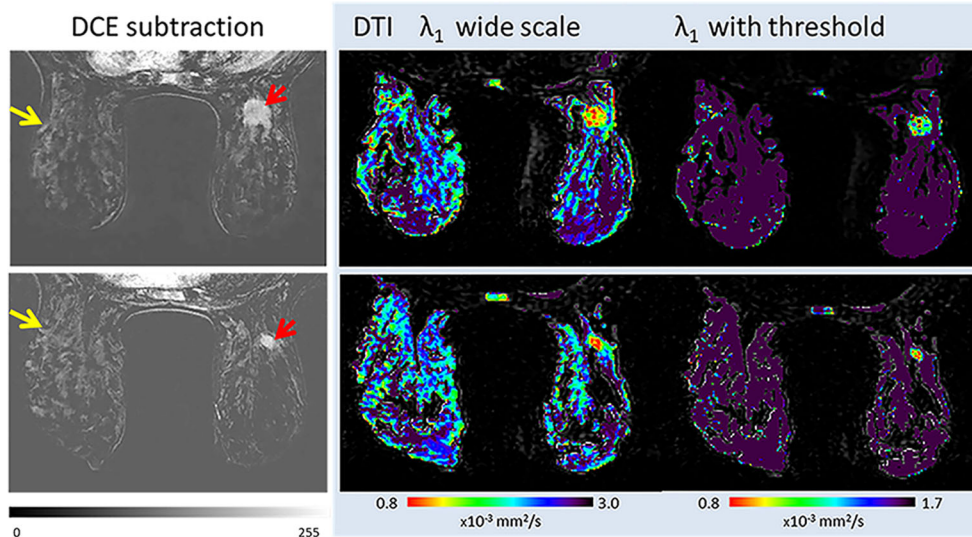


Fig. 4 DCE and λ_1 parametric maps of a lactating patient with multi-centric IDC. Representative images of a 30-year-old lactating patient with newly diagnosed multi-centric IDC: DCE subtraction images and DTI-derived λ_1 parametric maps of the two lesions are presented. The λ_1 maps are once presented with wide scale, where the complete spectrum of breast diffusivity is presented, and also with a parametric threshold, where pixels above the diffusivity threshold (with values $> 1.7 \times 10^{-3} \text{ mm}^2/\text{s}$) are colored in purple, whereas pixels below the threshold are colored

according to the parametric scale. The DCE image scale is in arbitrary units (0–255). The two lesions are visible in the DCE subtraction image (red arrowhead) on top of the apparent BPE (yellow arrow). On the wide-scale λ_1 maps, the tumor exhibits lower diffusivity compared with the normal lactating fibroglandular tissue. However, in the thresholded map, the tumor could be automatically discriminated from the normal surrounding tissue, enabling its straightforward segmentation

Fig. 5 DCE and λ_1 parametric map and mammography of tumor in a lactating patient with marked BPE. Representative images of a 37-year-old lactating patient who presented with palpable mass and was diagnosed with IDC: maximal intensity projection (MIP) and single-slice DCE subtraction images, DTI-derived λ_1 parametric map, and magnification view mammography are presented. The lesion is hardly visible on DCE subtraction images (red arrowhead) due to the marked BPE on both breasts (yellow arrow), which could be appreciated on the MIP view. A restricted diffusivity is apparent on λ_1 map in the tumor region, as was also confirmed by the scattered pleomorphic microcalcifications on mammography, which stresses the importance of multi-modality workup in such challenging cases

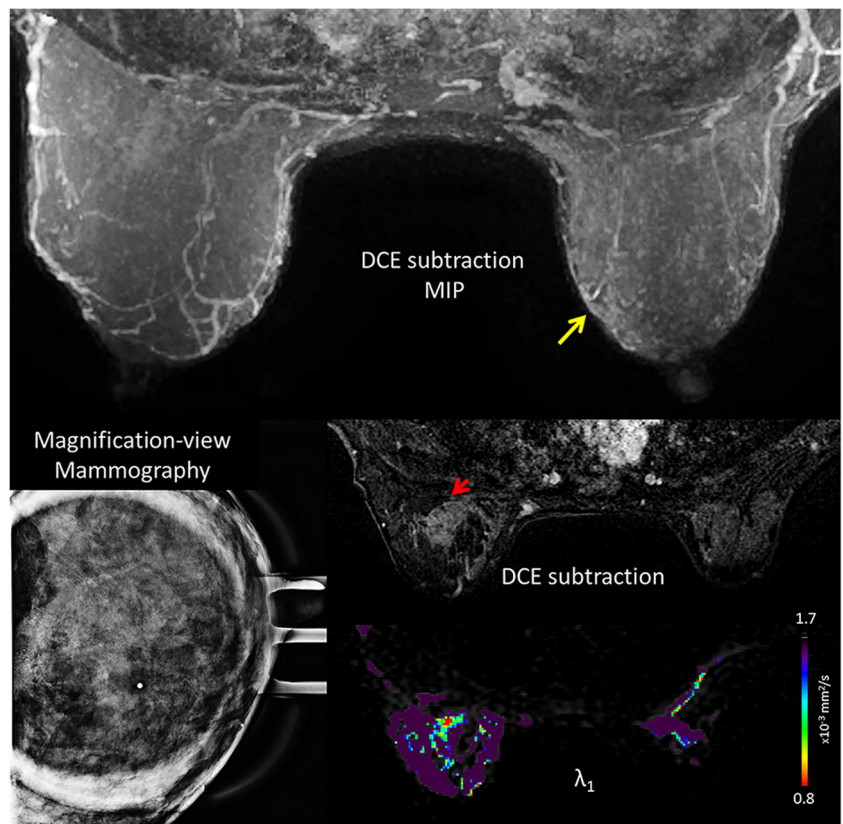
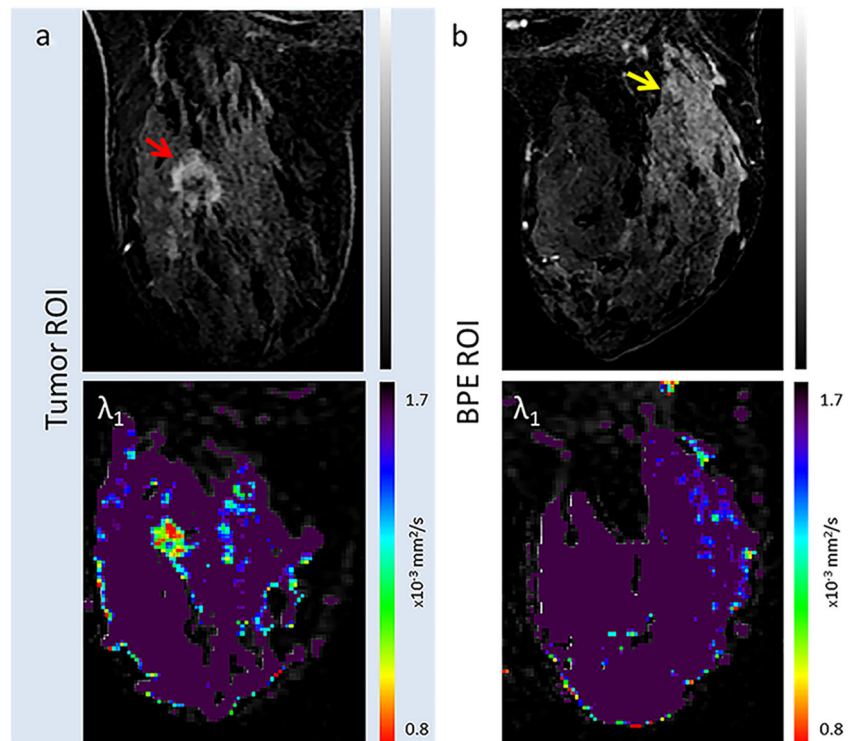


Fig. 6 DCE and λ_1 parametric maps of tumor and contralateral a marked BPE region. Representative images of a 34-year-old lactating patient with newly diagnosed IDC: DCE subtraction images and DTI-derived λ_1 parametric maps are presented for two ROIs: the tumor (left breast, left panel, marked by red arrowhead) and (b) a marked BPE region in the contralateral breast (right panel, yellow arrow). The lesion is visible in both the DCE subtraction image and in the λ_1 map. However, on the BPE region, except for scattered noisy pixels (especially at the tissue borders where partial volume effect exists), the λ_1 map exhibits normal diffusivity values, assisting in excluding contralateral disease



comparison with DCE. The anisotropy-derived parameters, λ_1 – λ_3 and FA, were found to provide significantly inferior CNR measurements compared with DCE, in both ROIs. Results are presented in Fig. 7.

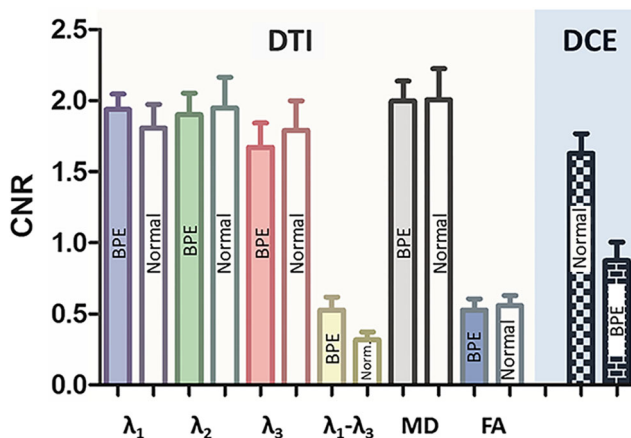


Fig. 7 CNR comparison between DTI parameters and DCE among lactating patients. CNR results of the lactating cohort are demonstrated in columns (mean \pm SD), for DTI parameters λ_1 , λ_2 , λ_3 , λ_1 – λ_3 , MD, and FA, as well as for DCE, when examined in comparison with the reciprocal (contralateral) normal fibroglandular tissue and to the most recognizable contralateral BPE region. Significantly higher mean CNR was measured for λ_1 , λ_2 , and MD compared with DCE, for the normal contralateral ROI ($p < 0.005$, $p < 0.5$, and $p < 0.005$, respectively). When measured in the BPE ROI, even higher differences were measured for λ_1 , λ_2 , λ_3 , and MD, comparing with DCE ($p < 0.0005$ for all). In both ROIs, the anisotropy indices exhibited significantly lower CNR than DCE

Discussion

Initiating in pregnancy, the mammary vasculature transformation and consequential drastic increase in the number of blood vessels evolve. In the first trimester, the mammary gland vessels give rise to numerous capillary sprouts, which grow rapidly, ramify, and anastomose with one another. Then, gradually, the amount of capillary sprouts decreases until it vanishes completely in advanced pregnancy stages, while in parallel, transcapillary pillar formation is developed [34]. An expansion of the vascular network progresses with increase in the cellular surface of the endothelial cells, as well as a dramatic increase in the number of mitochondria and pinocytotic vesicles, indicates high metabolic activity of the endothelium during lactation [34]. Ultimately, the fully differentiated lactating mammary gland is characterized with maximally developed endothelium, both morphologically and metabolically, in order to comply with the high imposed demands.

These physiologically dictated changes of vascular properties are clinically reflected in the form of the lactation-related-associated BPE phenomenon on breast DCE MRI, which was previously documented [7–10]. Here, we performed a retrospective case-control assessment of DCE datasets of lactating and non-lactating age-matched groups, in order to quantify the effect of lactation on breast cancer conspicuity. As anticipated, our results demonstrated and provided quantification of the marked reduction in tumor conspicuity in DCE MRI during lactation, stemming from the notable BPE of the lactating breast. Although this reduction does not automatically

translate to a reduction in breast cancer sensitivity [9], it supports the raised concerns regarding the role of breast DCE MRI during that period.

Preliminary DCE MRI breast studies during lactation suggested a possible capability to differentiate enhancing breast cancer from lactation-induced BPE based on kinetics and morphology [7–10], considering that the normal lactating breast exhibits a rapid enhancement on DCE followed by an early plateau of enhancement, owing to increased vascular permeability [10]. Myers et al reported on 12/53 (23%) additional biopsies indicated by DCE workup among PABC patients, which yielded four additional malignant foci (33%) [8]. Interestingly, Langer et al reported on three high-risk lactating patients who benefited from screening MRI which detected asymptomatic breast cancer [4]. Currently, guidelines support waiting until 3 months after cessation of breastfeeding, though screening breast MRI during lactation remains optional if a woman plans to breastfeed for a long period or is at very high risk for breast cancer [11].

Recently, several research groups have studied the diffusion properties of the breast during lactation. Sah et al reported on relatively decreased ADC values of the normal lactating fibroglandular tissue compared with the literature's normal range. Even though, the normal lactation ADC values were significantly higher than measurements of cancer among the non-lactating control group [35]. In agreement, a reduction of up to ~20% was reported for the DTI-derived diffusion coefficients of the lactating breast, which was attributed to the higher viscosity of the milk [22]. More recently, Iima et al reported on the intravoxel incoherent motion (IVIM) and non-Gaussian diffusion of the lactating breast, highlighting the increase in perfusion fraction and eventual changes post-weaning [36]. To our knowledge, this is the first report on the utility of diffusion-based breast MRI during lactation among breast cancer patients.

Previous DTI studies of the lactating breast showed a relative decrease in the diffusion coefficients that was attributed to the higher medium viscosity of the milk [22, 23]. Our preliminary results indicate that despite the observed reduced diffusivity in the normal lactating fibroglandular tissue, the diffusion coefficients remain significantly higher than those in cancer. Considering the reported range of DTI-derived diffusivity of breast cancer among non-lactating patients [15–17, 24–26, 29], as well as among pregnant patients [37], the observed diffusion-derived contrast comes without a surprise. Furthermore, our results suggest that the diffusion-derived contrast, in the form of CNR measurements, is even considerably higher than the DCE-derived tissue contrast. These encouraging results demonstrate the potential clinical utility of DTI breast examination as an effective adjunct diagnostic tool in pre-operative assessment of lactating patients and possibly in evaluation of symptomatic patients and screening of high-risk population during lactation.

DTI is a safe, rapid, and non-invasive methodology which dissects the breast architecture and can facilitate detection of breast cancer, especially in patients with a dense breast [38]. However, despite the observed advantage in the form of higher CNR, it currently holds two main setbacks compared with DCE: limited spatial resolution and technical robustness, through sensitivity to the presence of fat, EPI-related artifacts due to inhomogeneous magnetic and radiofrequency fields, eddy current-induced distortions, as well as tissue/air susceptibility differences and subject motion [39]. These drawbacks did not affect the cancer detectability in our cohort and were apparent to a lesser extent in this study, probably owing to high parenchymal density of the lactating breast, thus associated with better technical outcome [40]. Unlike during pregnancy, when DCE is prohibited and diffusion MRI must serve as a standalone modality [37], during lactation, the two modalities could be applied together as complementary methods.

The main limitation of this study is related to the fact that only extensive and palpable tumors were explored. The ability of DTI to depict more subtle forms of breast cancer remains questionable. Also, due to the rareness of lactating PABC and consequently our small cohort, a larger number of examinees are required to evaluate the diagnostic value of DTI, in terms of detection rate. Additionally, although out of the scope of this work, the high frequency of benign breast lesions during lactation [2] requires an assessment of the diagnosis accuracy using both DCE and DTI for the discrimination between benign and cancerous lesions.

In conclusion, the application of DTI may improve the visualization and quantitative characterization of PABC compared with DCE MRI which provides a limited conspicuity. We therefore suggest that DTI may possibly provide an added value in the diagnostic workup of PABC.

Acknowledgments NN thanks Prof. Hadassa Degani from the Weizmann Institute of Science for long hours of stimulating discussions, as well as for the permission to use the proprietary DTI software.

Funding information This study has received funding from The Israel Cancer Association and the Sheba Medical Center and Weizmann Institute of Science Research collaboration biomedical research grant.

Compliance with ethical standards

Guarantor The scientific guarantor of this publication is Dr. Noam Nissan.

Conflict of interest The authors of this manuscript declare no relationships with any companies, whose products or services may be related to the subject matter of the article.

Statistics and biometry One of the authors has significant statistical expertise.

Informed consent Written informed consent was obtained from all subjects (patients) in this study.

Ethical approval Institutional Review Board approval was obtained.

Methodology

- prospective
- case-control study/experimental
- performed at one institution, but patients were recruited in several centers

References

1. McManaman JL, Neville MC (2003) Mammary physiology and milk secretion. *Adv Drug Deliv Rev* 55:629–641
2. Vashi R, Hooley R, Butler R, Geisel J, Philpotts L (2013) Breast imaging of the pregnant and lactating patient: physiologic changes and common benign entities. *AJR Am J Roentgenol* 200:329–336
3. Andersson TM, Johansson AL, Hsieh CC, Cnattingius S, Lambe M (2009) Increasing incidence of pregnancy-associated breast cancer in Sweden. *Obstet Gynecol* 114(3):568–572
4. Langer A, Mohallem M, Stevens D, Rouzier R, Lerebours F, Chérel P (2014) A single-institution study of 117 pregnancy-associated breast cancers (pabc): presentation, imaging, clinicopathological data and outcome. *Diagn Interv Imaging* 95(4):435–441
5. Vashi R, Hooley R, Butler R, Geisel J, Philpotts L (2013) Breast imaging of the pregnant and lactating patient: imaging modalities and pregnancy-associated breast cancer. *AJR Am J Roentgenol* 200(2):321–328
6. Sardanelli F, Boetes C, Borisch B et al (2010) Magnetic resonance imaging of the breast: recommendations from the EUSOMA working group. *Eur J Cancer* 46(8):1296–1316
7. Oh SW, Lim HS, Moon SM et al (2017) MR imaging characteristics of breast cancer diagnosed during lactation. *Br J Radiol* 90(1078)
8. Myers KS, Green LA, Lebron L, Morris EA (2017) Imaging appearance and clinical impact of preoperative breast MRI in pregnancy-associated breast cancer. *AJR Am J Roentgenol* 209(3):W177–W183
9. Taron J, Fleischer S, Preibsch H, Nikolaou K, Gruber I, Bahrs S (2018) Background parenchymal enhancement in pregnancy-associated breast cancer: a hindrance to diagnosis? *Eur Radiol* 29(3):1187–1193
10. Espinosa LA, Daniel BL, Vidarsson L, Zakhour M, Ikeda DM, Herfkens RJ (2005) The lactating breast: contrast-enhanced MR imaging of normal tissue and cancer. *Radiology*. 237(2):429–436
11. diFlorio-Alexander RM, Slanetz PJ, Moy L et al (2018) ACR appropriateness criteria® breast imaging of pregnant and lactating women. *J Am Coll Radiol* 15(11S):S263–S275
12. Carmichael H, Matsen C, Freer P et al (2017) Breast cancer screening of pregnant and breastfeeding women with BRCA mutations. *Breast Cancer Res Treat* 162(2):225–230
13. Partridge SC, Nissan N, Rahbar H, Kitsch AE, Sigmund EE (2016) Diffusion-weighted breast MRI: clinical applications and emerging techniques. *J Magn Reson Imaging* 14:1–19
14. Partridge SC, Murthy RS, Ziadloo A, White SW, Allison KH, Lehman CD (2010) Diffusion tensor magnetic resonance imaging of the normal breast. *Magn Reson Imaging* 28(3):320–328
15. Eyal E, Shapiro-Feinberg M, Furman-Haran E et al (2012) Parametric diffusion tensor imaging of the breast. *Invest Radiol* 47(5):284–291
16. Baltzer PA, Schäfer A, Dietzel M et al (2011) Diffusion tensor magnetic resonance imaging of the breast: a pilot study. *Eur Radiol* 21(1):1–10
17. Partridge SC, Ziadloo A, Murthy R et al (2010) Diffusion tensor MRI: preliminary anisotropy measures and mapping of breast tumors. *J Magn Reson Imaging* 31(2):339–347
18. Le Bihan D, Mangin JF, Poupon C et al (2001) Diffusion tensor imaging: concepts and applications. *J Magn Reson Imaging* 13(4):534–546
19. Plaza MJ, Morris EA, Thakur SB (2016) Diffusion tensor imaging in the normal breast: influences of fibroglandular tissue composition and background parenchymal enhancement. *Clin Imaging* 40(3):506–511
20. Wiederer J, Pazahr S, Leo C, Nanz D, Boss A (2013) Quantitative breast MRI: 2D histogram analysis of diffusion tensor parameters in normal tissue. *MAGMA* 27(2):185–193
21. Teruel JR, Cho GY, Moccaldi Rt M et al (2017) Stimulated echo diffusion tensor imaging (STEAM-DTI) with varying diffusion times as a probe of breast tissue. *J Magn Reson Imaging* 45(1):84–93
22. Nissan N, Furman-Haran E, Shapiro-Feinberg M, Grobgeld D, Degani H (2014) Diffusion-tensor MR imaging of the breast: hormonal regulation. *Radiology*. 271(3):672–680
23. Nissan N, Furman-Haran E, Shapiro-Feinberg M, Grobgeld D, Degani H (2017) Monitoring in-vivo the mammary gland microstructure during morphogenesis from lactation to post-weaning using diffusion tensor MRI. *J Mammary Gland Biol Neoplasia* 22(3):193–202
24. Cakir O, Arslan A, Inan N et al (2013) Comparison of the diagnostic performances of diffusion parameters in diffusion weighted imaging and diffusion tensor imaging of breast lesions. *Eur J Radiol* 82(12):e801–e806
25. Teruel JR, Goa PE, Sjøbakk TE, Østlie A, Fjøsne HE, Bathen TF (2016) Diffusion weighted imaging for the differentiation of breast tumors: from apparent diffusion coefficient to high order diffusion tensor imaging. *J Magn Reson Imaging* 43(5):1111–1121
26. Onaygil C, Kaya H, Ugurlu MU, Aribal E (2017) Diagnostic performance of diffusion tensor imaging parameters in breast cancer and correlation with the prognostic factors. *J Magn Reson Imaging* 45(3):660–672
27. Kosmin M, Makris A, Joshi PV, Ah-See ML, Woolf D, Padhani AR (2017) The addition of whole-body magnetic resonance imaging to body computerised tomography alters treatment decisions in patients with metastatic breast cancer. *Eur J Cancer* 77:109–116
28. Furman-Haran E, Grobgeld D, Nissan N, Shapiro-Feinberg M, Degani H (2016) Can diffusion tensor anisotropy indices assist in breast cancer detection? *J Magn Reson Imaging* 44(6):1624–1632
29. Tsougos I, Bakosis M, Tsivaka D et al (2019) Diagnostic performance of quantitative diffusion tensor imaging for the differentiation of breast lesions at 3 T MRI. *Clin Imaging* 53:25–31
30. Wilmes LJ, Li W, Shin HJ et al (2016) Diffusion tensor imaging for assessment of response to neoadjuvant chemotherapy in patients with breast cancer. *Tomography*. 2(4):438–447
31. Furman-Haran E, Nissan N, Ricart-Selma V, Martinez-Rubio C, Degani H, Camps-Herrero J (2017) Quantitative evaluation of breast cancer response to neoadjuvant chemotherapy by diffusion tensor imaging: initial results. *J Magn Reson Imaging* 47(4):1080–1090
32. Bogner W, Gruber S, Pinker K et al (2009) Diffusion-weighted MR for differentiation of breast lesions at 3.0 T: how does selection of diffusion protocols affect diagnosis? *Radiology*. 253(2):341–351

33. Partridge SC, Singer L, Sun R et al (2011) Diffusion-weighted MRI: influence of intravoxel fat signal and breast density on breast tumor conspicuity and apparent diffusion coefficient measurements. *Magn Reson Imaging* 29(9):1215–1221
34. Djonov V, Andres AC, Ziemiecki A (2001) Vascular remodelling during the normal and malignant life cycle of the mammary gland. *Microsc Res Tech* 52(2):182–189
35. Sah RG, Agarwal K, Sharma U, Parshad R, Seenu V, Jagannathan NR (2015) Characterization of malignant breast tissue of breast cancer patients and the normal breast tissue of healthy lactating women volunteers using diffusion MRI and in vivo ¹H MR spectroscopy. *J Magn Reson Imaging* 41(1):169–174 36
36. Iima M, Kataoka M, Sakaguchi R et al (2018) Intravoxel incoherent motion (IVIM) and non-Gaussian diffusion MRI of the lactating breast. *Eur J Radiol Open* 5:24–30
37. Nissan N, Furman-Haran E, Allweis T et al (2018) Noncontrast breast MRI during pregnancy using diffusion tensor imaging: a feasibility study. *J Magn Reson Imaging* 49(2):508–517
38. Nissan N, Furman-Haran E, Feinberg-Shapiro M et al (2014) Tracking the mammary architectural features and detecting breast cancer with magnetic resonance diffusion tensor imaging. *J Vis Exp* (94):1–18
39. Furman-Haran E, Eyal E, Shapiro-Feinberg M et al (2012) Advantages and drawbacks of breast DTI. *Eur J Radiol* 81:S45–S47
40. Shapiro-Feinberg M, Weisenberg N, Zehavi T et al (2012) Clinical results of DTI. *Eur J Radiol* 81(1):S151–152. [https://doi.org/10.1016/S0720-048X\(12\)70063-3](https://doi.org/10.1016/S0720-048X(12)70063-3)

Publisher's note Springer Nature remains neutral with regard to jurisdictional claims in published maps and institutional affiliations.